Science Translational Medicine
AAAS

Supplementary Materials for

Calreticulin mutant myeloproliferative neoplasms induce MHC-I skewing, which can be overcome by an optimized peptide cancer vaccine

Mathieu Gigoux *et al.*

Corresponding author: Mathieu Gigoux, gigouxm@mskcc.org; Taha Merghoub, merghout@mskcc.org

Sci. Transl. Med. **14**, eaba4380 (2022)
DOI: 10.1126/scitranslmed.aba4380

The PDF file includes:

Figs. S1 to S14

Other Supplementary Material for this manuscript includes the following:

Tables S1 to S12
Data file S1
MDAR Reproducibility Checklist

Supplementary Materials
Gigoux *et al.*

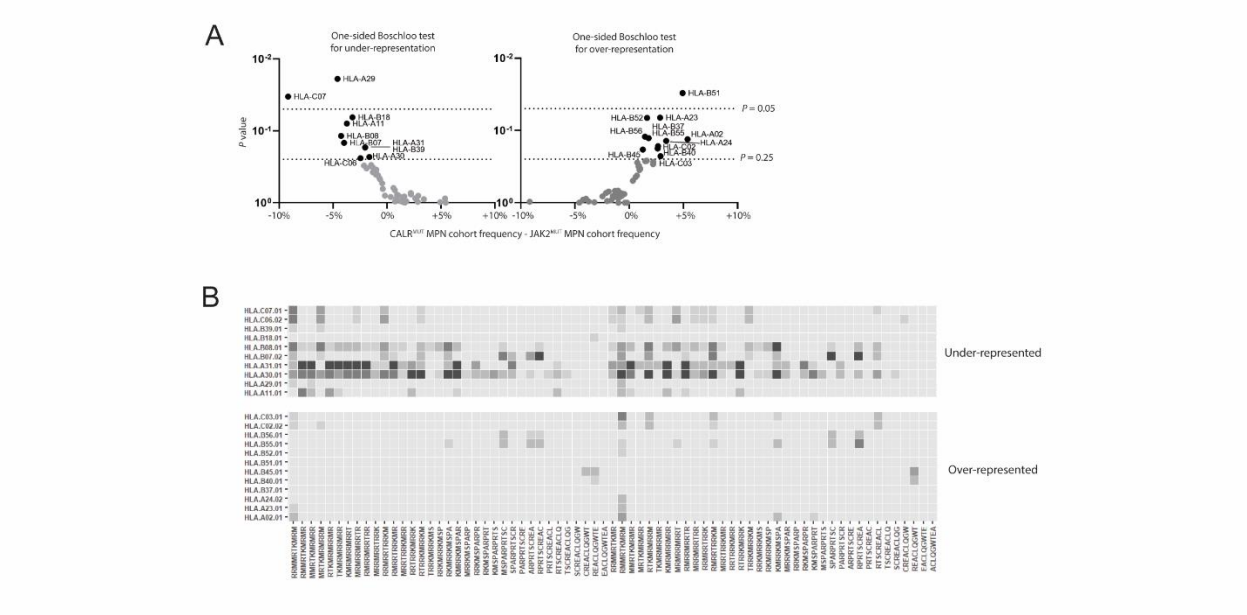

Fig. S1. MHC-I allele group skewing by Boschloo test. A) Volcano plots representing significance and difference in frequency between MHC-I allele groups from $CALR^{MUT}$ and $JAK2^{MUT}$ MPN cohorts as calculated by one-side contingency Boschloo tests. B) Heatmap of NetMHCpan v 3.0 predicted binding affinity of each $CALR^{MUT}$-derived peptide to a representative MHC-I allele from the under- or over-represented MHC-I allele groups ($P < 0.25$ cutoff) from *A*.

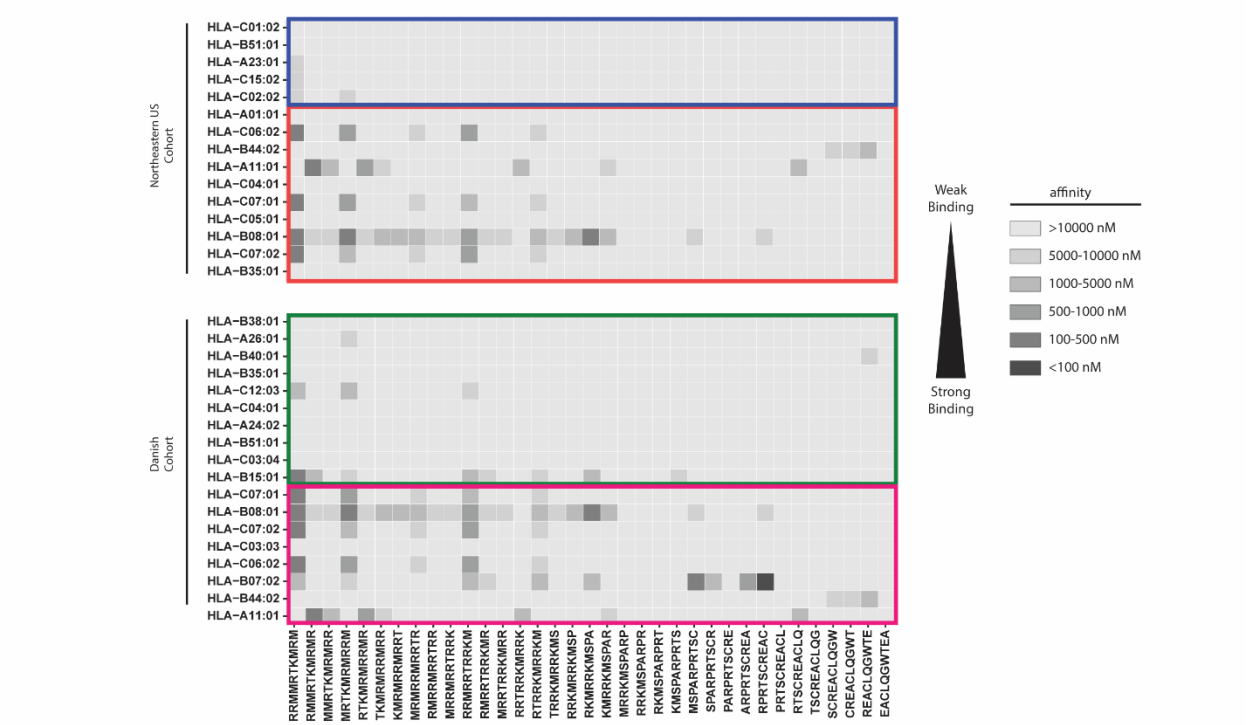

Fig. S2. MHC-I alleles with predicted binding to CALR^{MUT}-derived peptides are less frequent in CALR^{MUT} MPNs. Heatmap of predicted binding to each CALR^{MUT}-derived 10mer peptide to each differentially expressed MHC-I allele. Colored boxes represent MHC-I alleles more frequent (blue for NEUS cohort and green for Danish cohort) and less frequent (red for NEUS cohort and pink for Danish cohort) in CALR^{MUT} MPN patients.

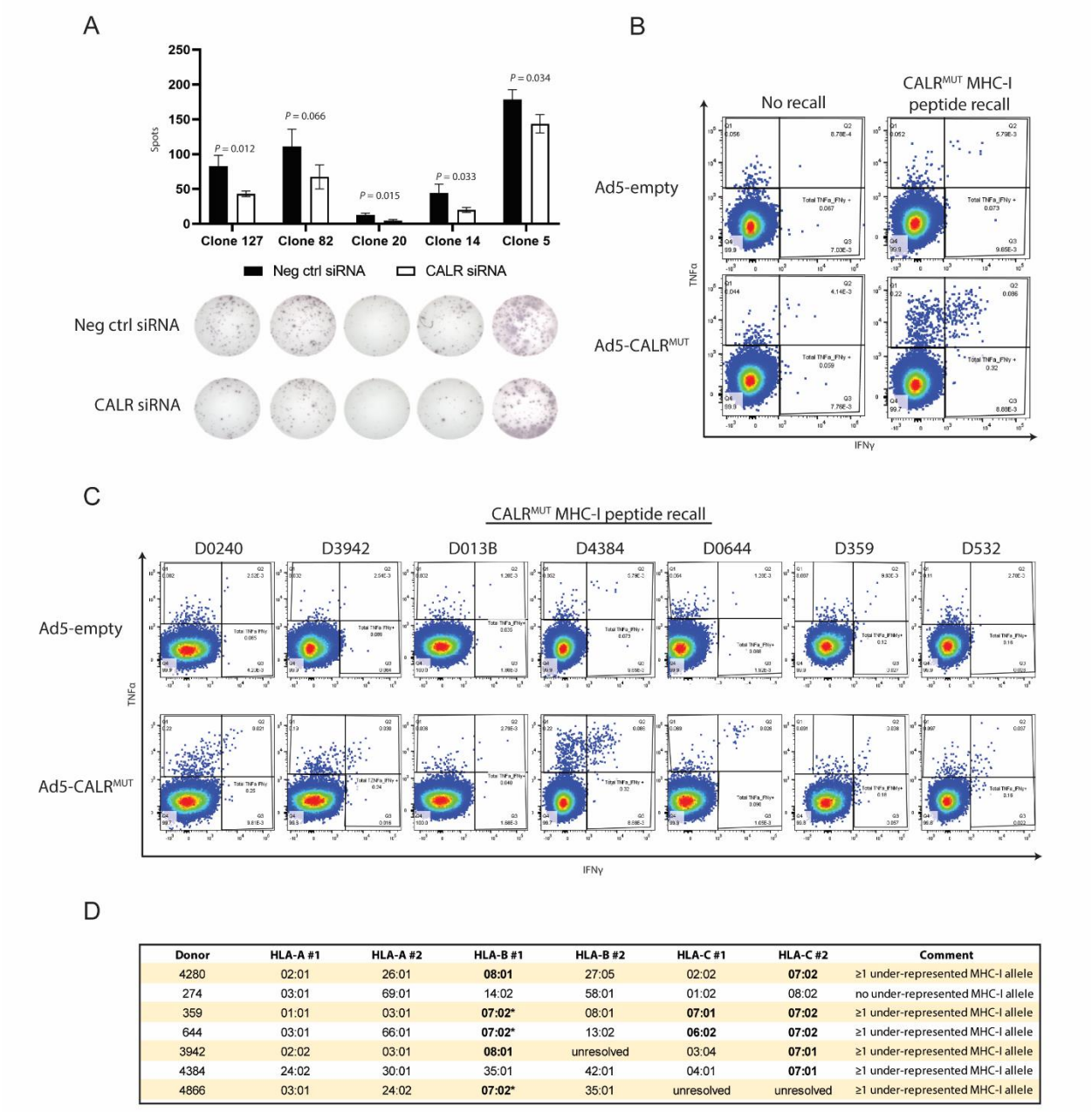

Donor	HLA-A #1	HLA-A #2	HLA-B #1	HLA-B #2	HLA-C #1	HLA-C #2	Comment
4280	02:01	26:01	**08:01**	27:05	02:02	**07:02**	≥1 under-represented MHC-I allele
274	03:01	69:01	14:02	58:01	01:02	08:02	no under-represented MHC-I allele
359	01:01	03:01	**07:02***	08:01	**07:01**	**07:02**	≥1 under-represented MHC-I allele
644	03:01	66:01	**07:02***	13:02	**06:02**	**07:02**	≥1 under-represented MHC-I allele
3942	02:02	03:01	**08:01**	unresolved	03:04	**07:01**	≥1 under-represented MHC-I allele
4384	24:02	30:01	35:01	42:01	04:01	**07:01**	≥1 under-represented MHC-I allele
4866	03:01	24:02	**07:02***	35:01	unresolved	unresolved	≥1 under-represented MHC-I allele

Fig. S3. The full length CALR^{MUT} antigen is endogenously processed and presented in human cells. A) The CALRLong36 specific CD8^{+} T cells described above were assayed in an IFNγ ELISpot with CALR^{MUT}-positive CD14^{+} monocytes that had been transfected with either CALR siRNA or negative control siRNA. B) Representative result of human CD8^{+} T cells activated with primary myeloid cells infected with either Ad5-empty or Ad5-CALR^{MUT}, and subject to a recall using no peptides or a peptide pool consisting of peptides derived from the 44 amino-acid CALR^{MUT} fragment followed by IFNγ and TNFα intracellular staining. C) Flow cytometry results following CALR^{MUT} MHC-I pool recall of healthy PBMC donor previously activated using Ad5-CALR^{MUT} infected autologous myeloid cells. Only showing results from the 7 of 20 healthy donors that exhibited a positive result (>0.01% and 3-fold over background). Gated on live CD8^{+} T cells. D) MHC-I allele haplotypes of the 7 healthy donors that had a

$CALR^{MUT}$-specific secondary reactivity following Ad5-$CALR^{MUT}$ priming. Bolded alleles represent those previously identified as under-represented in $CALR^{MUT}$ MPN patients from Fig 2. The * denotes the HLA-B*07:02 allele, which was under-represented in the Danish cohort but did not reach the threshold in the NEUS cohort.

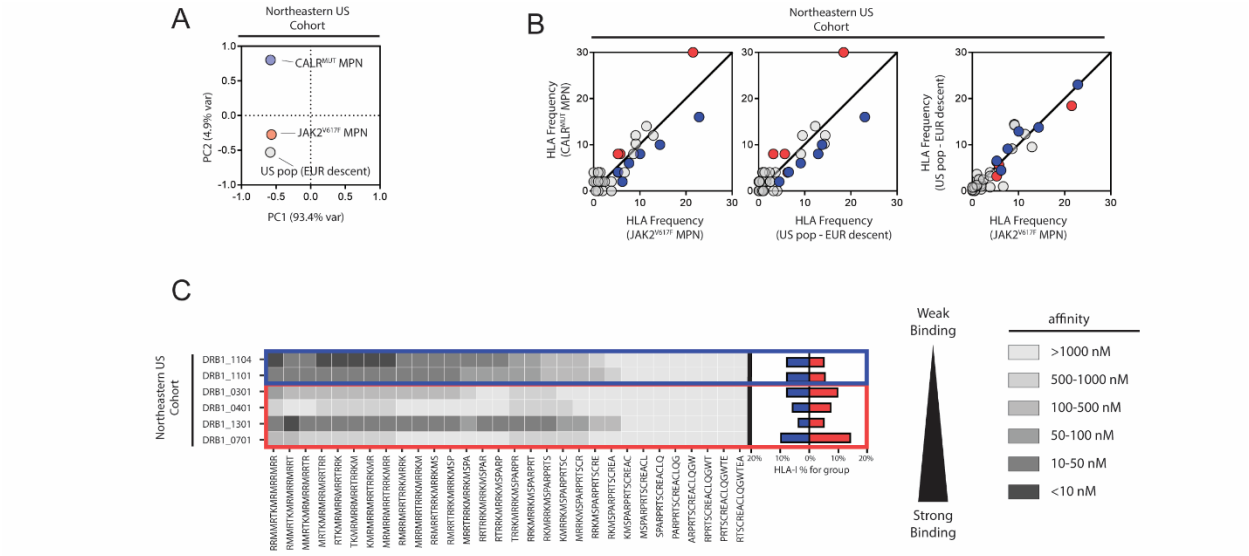

Fig. S4. MHC-II alleles skewing in CALR^{MUT} MPN patients compared to JAK2^{V617F} MPN patients from NEUS cohort. A) Principal component analysis of HLA-II allele frequencies from CALR^{MUT} MPN patients, JAK2^{V617F} MPN patients and US Caucasian population. B) Comparison of MHC-II allele frequencies from each group compared to each other in NEUS cohort. MHC-II alleles with greater (depicted as red dots) or lesser (depicted as blue dots) are shown here. Exact values are listed in Supplementary Table 8. Only MHC-II alleles differentially expressed between CALR^{MUT} MPN patients compared to both JAK2^{V617F} MPN patients and US Caucasian population were considered. C) Heatmap of predicted binding to each CALR^{MUT}-derived 15mer peptide to each differentially expressed MHC-II allele. Colored boxes represent MHC-I alleles more frequent (blue) and less frequent (red) in CALR^{MUT} MPN patients.

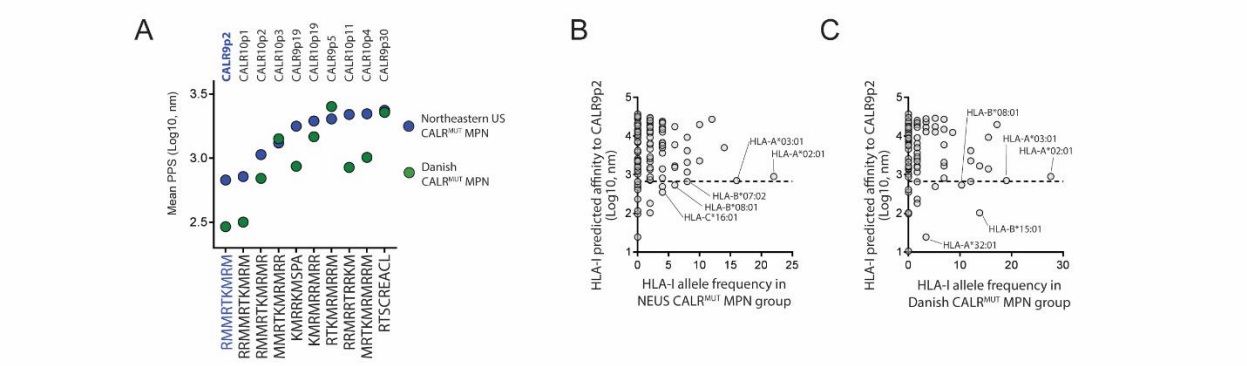

Fig. S5. Identification of strongest MHC-I binding CALRMUT minimal epitope in CALR^{MUT} MPN patients. A) Top ten best predicted mean PPS of CALR^{MUT} MPN patients. Peptide sequences are labeled below and shorthand code (CALR-length-p-start position) are identified above. B) Breakdown of MHC-I allele frequencies in CALR^{MUT} MPN patients from NEUS cohort or C) Danish cohort, versus the predicted binding affinity to the top peptide CALR9p2.

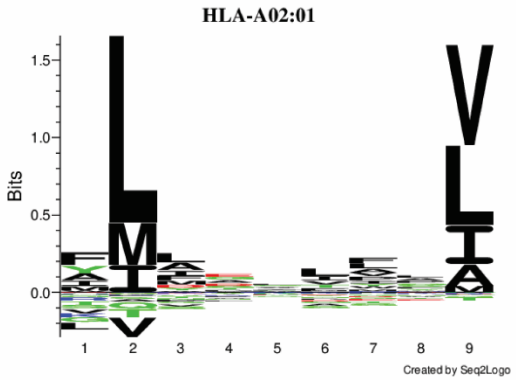

Fig. S6. NetMHCpan 3.0 Seq2Logo sequence binding motifs of HLA-A*02:01. Amino acid binding motif of HLA-A*02:01 binding peptide. This graph was plotted using the Sequence Motif function of the online portal. The numbers on the x-axis indicate the amino acid position, and the values of the y-axis represent the relative enrichment of the specific amino acids at those positions. Positive values represent favorable binding and negative blues present unfavorable binding.

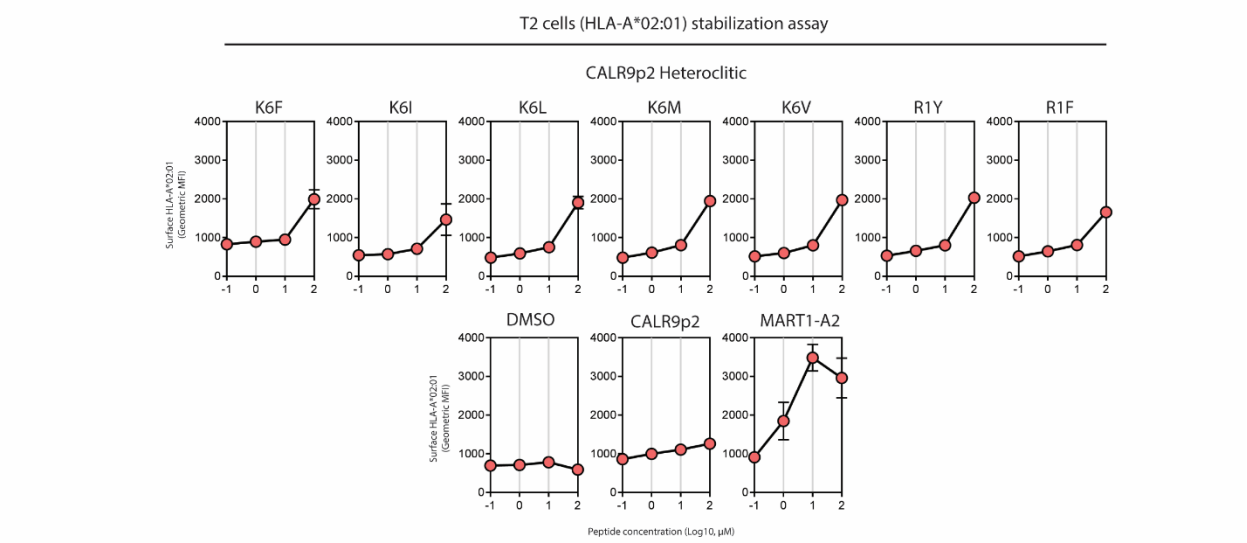

Fig. S7. CALR9p2 heteroclitic peptides increase HLA-A*02:01 stabilization compared to CALR9p2. MHC-I stabilization assay using human TAP-deficient T2 cells was performed for CALR9p2 and CALR9p2 heteroclitic peptides. The MART1-A2 peptide was used as a positive control.

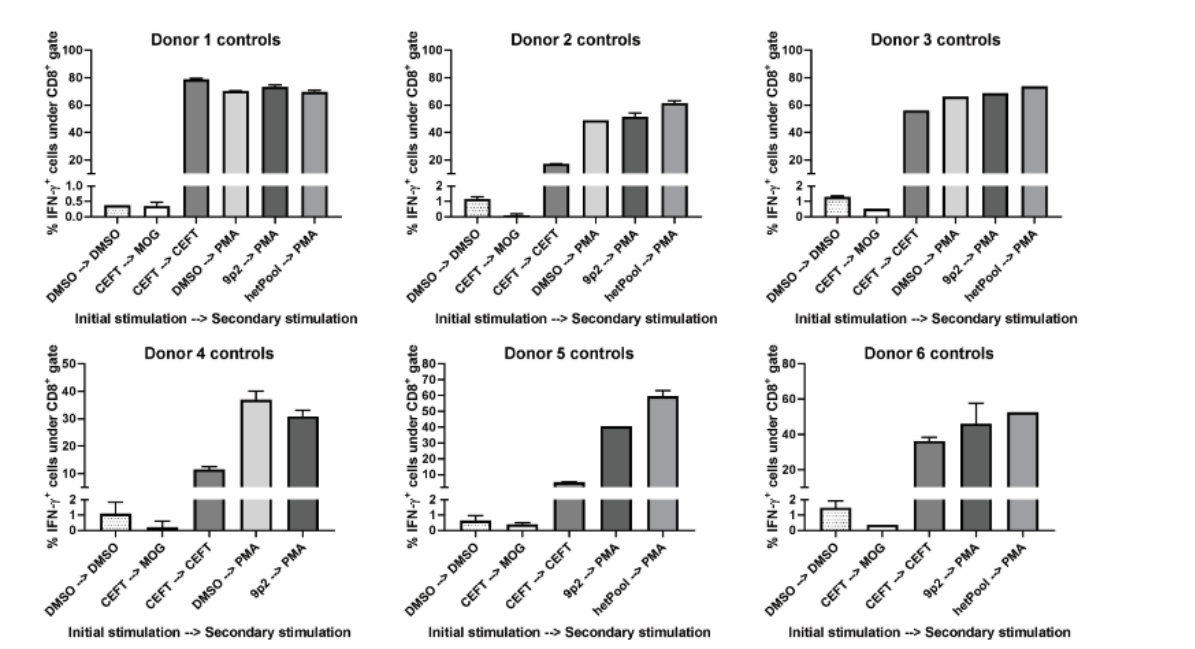

Fig. S8. Control secondary stimulatory conditions of rapid T cell assay of human healthy donor PBMCs. Graphed results of secondary stimulation MOG, CEFT and PMA + Ionomycin (PMA), of human healthy donors that had received the initial stimulation of DMSO, CEFT, CALR9p2 (9p2) and all pool heteroclitic peptides (hetPool). In some cases, not all conditions could be tested.

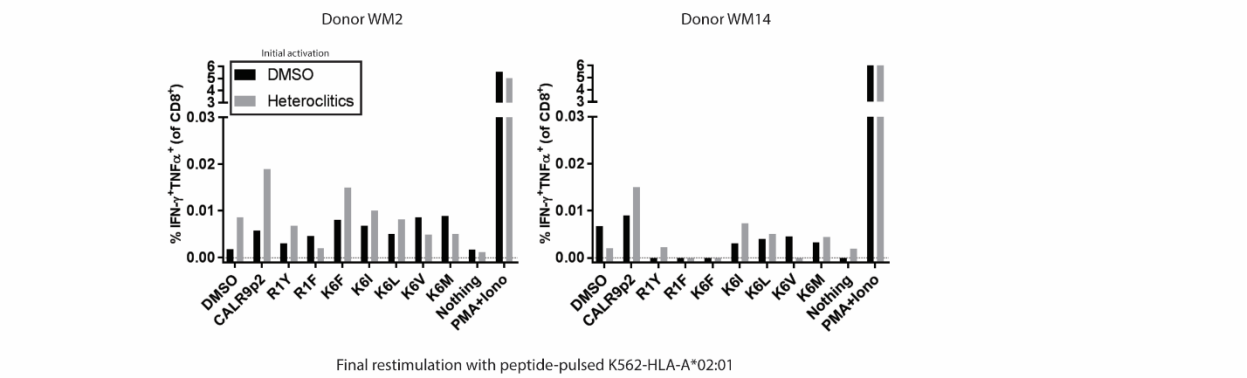

Fig. S9. CALR9p2 heteroclitic peptides can mount cross-reactive response to CALR9p2 through HLA-A*02:01. PBMCs from two healthy donors were activated in vitro with CALR9p2 heteroclitic peptides and final restimulation was provided by peptide-pulsed HLA-A*02:01-transduced K562 cells. Reactivity was assessed by intracellular staining for IFNγ and TNFα by flow cytometry.

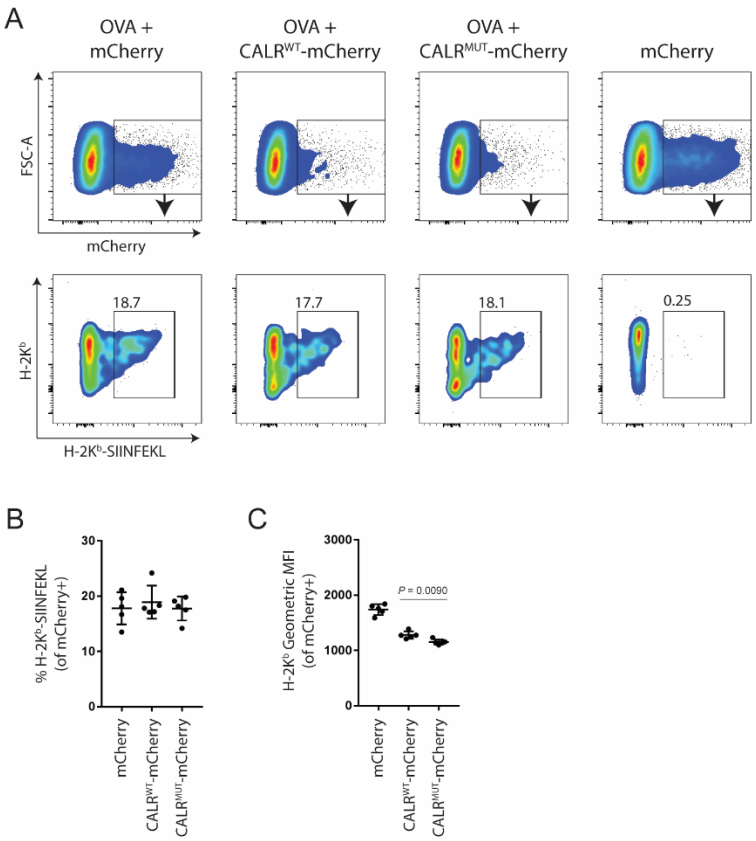

Fig. S10. CALR^{MUT} does not inhibit antigen processing and presentation. A) Representative flow cytometry image of B16F10 cells presentation of SIINFEKL bound to H-2K^b following co-transfection with OVA and different CALR constructs. B) Quantification of the percentage of B16F10 cells presenting SIINFEKL H-2K^b and C) total expression of H-2K^b. Data shown represent results from one repeat of experiments performed at least three times. A Student's *t* test was used to determine significance.

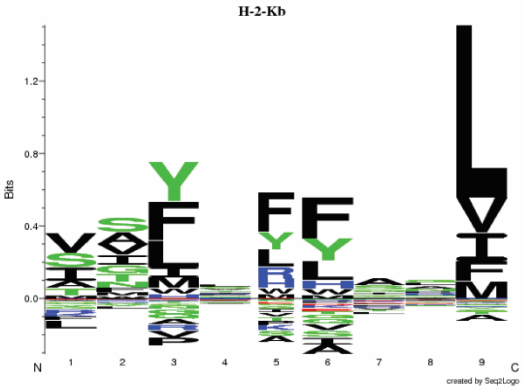

Fig. S11. NetMHC 4.0 Seq2Logo sequence binding motifs of H-2K^{b}. Amino acid binding motif of H-2K^{b} binding peptide. This graph was plotted using the Sequence Motif function of the online portal. The numbers on the x-axis indicate the amino acid position, and the values of the y-axis represent the relative enrichment of the specific amino acids at those positions. Positive values represent favorable binding and negative blues present unfavorable binding.

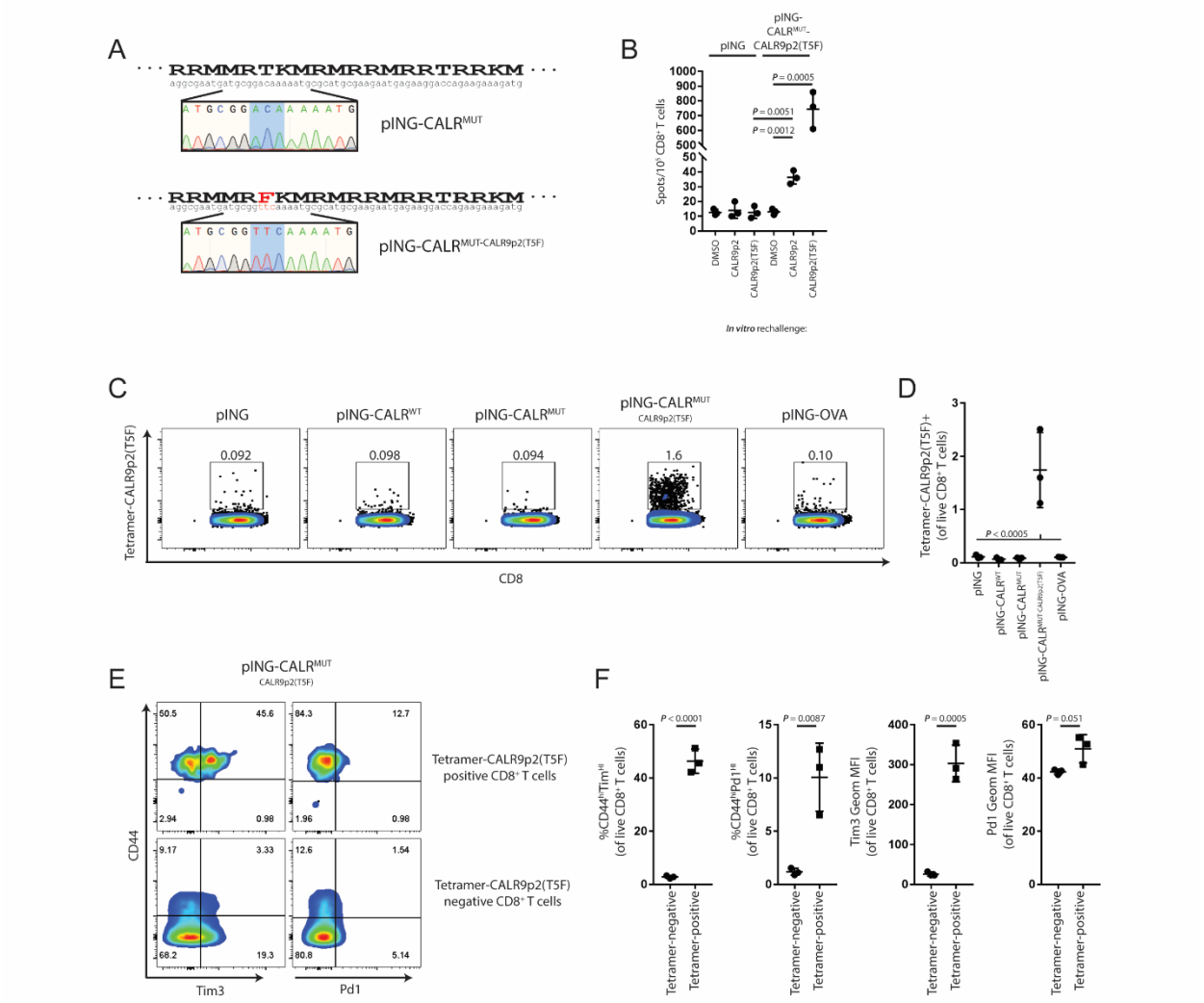

Fig. S12. Full-length CALR^{MUT} encoding CALR9p2(T5F) elicits activated antigen-specific CD8$^+$ T cells. A) Depiction and Sanger sequencing validation of site-directed mutagenesis introducing CALR9p2(T5F) variant in the pING-CALR^{MUT} DNA vaccine sequence. Only relevant section of DNA construct is depicted. B) IFNγ ELISpot following co-culture of CD8$^+$ T cells from dLNs of pING or pING-CALR$^{MUT\text{-}CALR9p2(T5F)}$-immunized mice with peptide-pulsed T cell-depleted splenocytes. C) Representative image of CALR9p2(T5F)-tetramer staining of live CD8$^+$ T cells from spleen. D) Quantification of CALR9p2(T5F)-tetramer-positive live CD8$^+$ T cells from *C)*. E) Representative image of the surface expression of Cd44, Tim3 and Pd1 on CALR9p2(T5F)-tetramer-negative and -positive live CD8$^+$ T cells from spleen of pING-CALR$^{MUT\text{-}CALR9p2(T5F)}$-immunized mice. F). Quantification of CD44^{HI}Tim3^{HI} and CD44^{HI}Pd1^{HI}, as well as geometric MFI of Tim3 and Pd1 of CALR9p2(T5F)-tetramer-negative and -positive live CD8$^+$ T cells from pING-CALR$^{MUT\text{-}CALR9p2(T5F)}$-immunized mice from *E)*. Showing one of two representative experiments. Statistical significance was calculated using the Student *t* test.

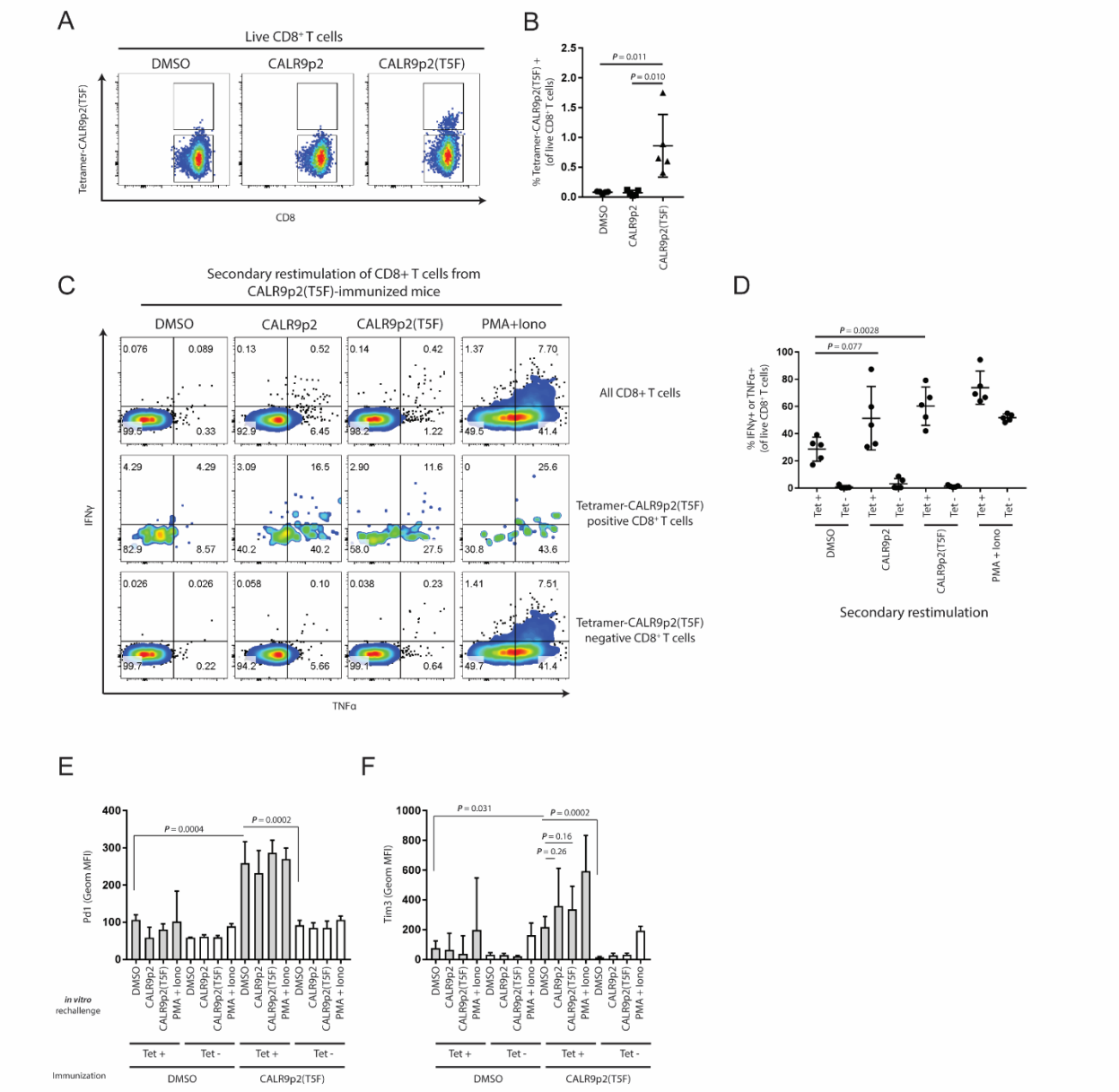

Fig. S13. Demonstration that CALR9p2(T5F)-specific CD8$^+$ T cells also recognize CALR9p2 following in vitro secondary restimulation. A) Representative image of CALR9p2(T5F)-tetramer staining on live CD8$^+$ T cells from dLNs of d7 peptide-immunized mice. Samples shown are from secondary control restimulation of DMSO-pulsed splenocytes. B) Quantification of live CD8$^+$ T cells CALR9p2(T5F)-tetramer staining from *A)*. C) Representative image of IFNγ and TNFα intracellular staining following secondary restimulation with peptide-pulsed splenocytes or PMA/Ionomycin of all, CALR9p2(T5F)-tetramer negative, or CALR9p2(T5F)-tetramer positive live CD8$^+$ T cells from CALR9p2(T5F) peptide-immunized mice. D) Quantification of live CD8$^+$ T cells for IFNγ or TNFα positivity in CALR9p2(T5F)-tetramer negative or positive CD8$^+$ T cells from *C)*. E-F) Quantification of E) Pd1 and F) Tim3 surface expression by flow cytometry of CALR9p2(T5F)-tetramer negative or positive of live

$CD8^+$ T cells from CALR9p2(T5F)-immunized mice restimulated with splenocytes-pulsed with indicated peptides or PMA/Ionomycin. To control for possible staining artifacts, also showing results from background stained CALR9p2(T5F)-tetramer negative or positive live $CD8^+$ T cells from DMSO-immunized mice. Experiment shown is representative of experiment performed twice. Statistical significance was calculated using the Student *t* test.

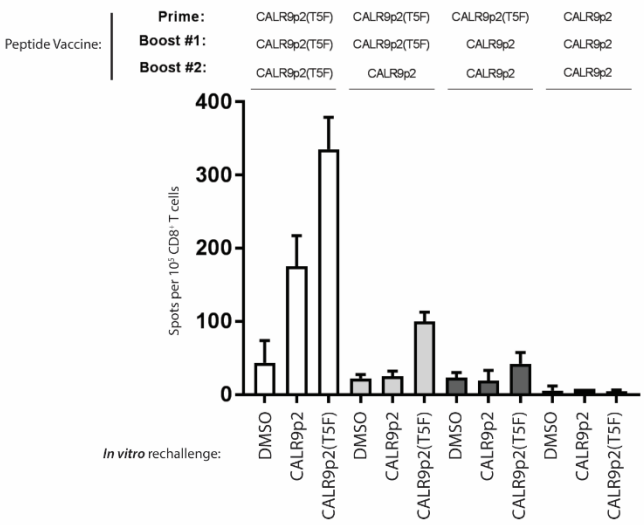

Fig. S14. CALR9p2 cross-reactivity of CD8$^+$ T cells primed by CALR9p2(T5F) diminishes over time and is not maintained by subsequent CALR9p2 boosts. IFNγ ELISpot depicting secondary restimulation of CD8$^+$ T cells isolated from draining lymph nodes of hock peptide-immunized at different timepoints. Boost #1 and Boost #2 occur at days 7 and 14, respectively.